

Modulation of an optical needle's reflectivity alters the average photon path through scattering media

Paul Simonson
Enrico D'Amico
Enrico Gratton

University of Illinois at Urbana-Champaign
Department of Physics
Laboratory for Fluorescence Dynamics, MC-704
1110 West Green Street
Urbana, Illinois 61801-3080
E-mail: psimonso@uiuc.edu

Abstract. We introduce the concept of deliberate placement of absorbers to alter the average path of photons through tissue for a biomedical optical device. By changing the reflectivity of a needle that separates a source and detector, the average photon path through a turbid medium can be changed. Totally reflective needles have photon scattering density functions similar to a point source and detector in an infinite medium. An absorbing needle moves the average photon path of photons that reach the detector away from the needle. Thus, by modulating the reflectivity of the needle, it is possible to modify the sensitive volume, and simple tomography data should be possible. These results are confirmed by Monte Carlo simulations and experiment. Experiments include moving a black target relative to an optical "needle" and measuring the resulting intensity and phase lag of light reaching a detector at the distal end of the needle. © 2006 Society of Photo-Optical Instrumentation Engineers. [DOI: 10.1117/1.2168167]

Keywords: needle; reflectivity; Monte Carlo simulation; diffusion approximation; turbid media.

Paper 04212RR received Nov. 5, 2004; revised manuscript received Sep. 27, 2005; accepted for publication Oct. 19, 2005; published online Jan. 31, 2006.

1 Introduction

Optical biopsy needles are currently being investigated by Lubawy and Ramanujam for use in breast cancer diagnosis.¹ These needles offer the advantages of being real-time and minimally invasive probes that offer detailed descriptions of breast tissue. Diagnosis is virtually immediate, and accuracy is reported to be greater than 90%.

These needles consist of hollow biopsy needles threaded with optical fibers. At one end of the needle, light is emitted from a source optical fiber.¹ Light is multiply scattered through breast tissue until it enters the detector optical fiber at the distal end of the biopsy needle.¹ These optical needles have simple, fixed geometries that have one defining average photon path and, as shown here, a relatively small measurement volume.

In this paper, we investigate how changing the reflectivity of a needle between the source and detector alters the average photon path through a turbid medium. We demonstrate that by decreasing the reflectivity of the needle, the average photon path through the turbid medium is effectively shifted away from the needle. This is due to the fact that photons that travel near to and collide with the needle are absorbed. These absorbed photons do not contribute to the average path of photons that reach the detector, which in turn shifts the average path that photons travel in reaching the detector away from the needle. The ability to modify the average photon path is significant because, if it is possible to control the volume of tissue that photons visit, simple tomography using optical needles is possible. Because of the cylindrical symmetry of

the needle, it is possible to differentiate volumes at different distances away from the black needle but not volumes rotated around the principal axis of the needle; hence the qualification "simple tomography."

We use diffusion theory, Monte Carlo simulations, and experiment to investigate the change in average photon paths. We begin by using diffusion approximation theory after the manner of Patterson et al.² to construct photon density functions. These photon density functions describe the probability that a photon visits a point in space \mathbf{r}' and eventually reaches a detector, all the while not being absorbed by the needle. We define probability functions by modeling the end of the source optical fiber as an isotropic point source in a turbid, infinite medium. We model the optical needle as a negative line segment source; its intensity along the length of the needle is dependent on its distance away from the point source. The Green's functions of these two sources are used to calculate the relative probability that photons pass through a point \mathbf{r}' relative to the absorbing needle and constitute the first probability function. A similar Green's function is used to calculate the relative probability that photons leaving \mathbf{r}' reach the detector, giving our second probability function. Then, the photon density function is the product of these two probabilities. Numerical methods are used to produce 2-D images demonstrating these photon density functions.

Next, we use Monte Carlo simulations to construct photon scattering density functions (PSDFs) using methods outlined by Bevilacqua et al.³ and Wang et al.⁴ Monte Carlo PSDFs should be considered more correct than the functions obtained from our diffusion approximations because (1) they are accurate in both the diffusive and nondiffusive regimes,³ and (2)

Address all correspondence to Paul Simonson, Physics, University of Illinois at Urbana-Champaign, Lab. for Fluor. Dyn., Dept. Physics, MC-704, 1110 W. Green St., Urbana, IL 61801-3080.

they model the needle as a hard shell cylinder with a defined radius, rather than as an infinitely thin line segment source. We use the simulations to explore the effect that changing the needle reflectivity produces on the PSDFs, as well as demonstrating how moving an inhomogeneity through the turbid medium near the needle changes the intensity of light arriving at the detector.

Finally, we use the methods outlined by Patterson et al.² to experimentally produce images that relate to the photon density functions and PSDFs obtained using diffusion theory and Monte Carlo simulations. We use a blackened optical fiber immersed in milk to simulate an absorbing needle in scattering tissue. A small, black target is used to probe the photon density near the "needle." We also collect frequency domain information that demonstrates how the phase lag of light reaching the detector changes as a function of the position of the black target. The images produced correlate with our predictions from diffusion approximation and Monte Carlo simulations.

We end with a discussion of the significance of this experiment for biomedical optics, especially for optical breast cancer diagnosis.

2 Diffusion Approximations

In this paper, we derive only dc diffusion approximations for the cylindrical geometry of the needle. We consider the diffusion approximations for our work as giving an idea of what the geometry of the photon paths should look like. For calculations of the photon paths for this geometry that are accurate in both the diffusive and nondiffusive regimes and are calculated in the frequency domain, Monte Carlo simulations are the method of choice. For diffusion approximation derivations in the frequency domain in the presence of a cylindrical inhomogeneity, we refer to Walker et al.⁵

The diffusion equation has been used to predict with good results the migration of photons through turbid media.^{2,3,6-11} The diffusion equation is a good approximation for media in which $\mu_s \gg \mu_a$ and for distances away from sources, boundaries, and detectors that are much greater than the mean free path for light scattering.⁵ Although this paper does not suggest a solution to the diffusion equation for the black needle geometry (we use a line segment to model the needle), it does make qualitative predictions about the migration of photons in the absorbing needle geometry.

Light propagation in turbid media is modeled by linear transport theory using the diffusion approximation equations^{6,7}

$$\frac{\partial U(\mathbf{r}, t)}{\partial t} + v\mu_a U(\mathbf{r}, t) + \nabla \cdot \mathbf{J}(\mathbf{r}, t) = q_0(\mathbf{r}, t), \quad (1a)$$

$$\nabla U(\mathbf{r}, t) + \frac{3\partial \mathbf{J}(\mathbf{r}, t)}{v^2 \partial t} + \frac{\mathbf{J}(\mathbf{r}, t)}{vD} = 0, \quad (1b)$$

where $U(\mathbf{r}, t)$ is the density of photons, $\mathbf{J}(\mathbf{r}, t)$ is the photon current density, v is the speed of light in the medium, D is the diffusion coefficient, μ_a is the absorption coefficient, and μ_s is the scattering coefficient; but the diffusion equation can only be solved for a limited number of geometries.^{1,2} Solutions to the diffusion equation have been found for infinite

media, semiinfinite media bounded by a plane, a semiinfinite plane immersed in an infinite medium, and so forth, where the geometries of the boundary conditions are relatively simple.^{5-7,12,13} In the case of semiinfinite slabs, the diffusion equation is solved by introducing images that counteract the sources so as to produce a planar boundary where the photon fluence is zero.^{2,6,7} However, the geometry of the black needle problem does not lend itself well to the method of images. An analogous image method that creates a boundary corresponding to the radius of the black needle is apparently not possible. We do, however, model the absorbing needle as a negative source of photons.

For the absorbing needle problem, the probability that a photon visits a volume dV at \mathbf{r}' and goes on to the detector is the product of two probability functions.^{2,3} The first is the probability that a photon is emitted from the source at \mathbf{r}_0 and reaches \mathbf{r}' , and it is given by $P(\mathbf{r}_0 \rightarrow \mathbf{r}')$. The second is the probability that a photon leaves \mathbf{r}' and reaches the detector at \mathbf{r}_d and is given by $P(\mathbf{r}' \rightarrow \mathbf{r}_d)$. Calculating the probability that a photon visits a given region of space before detection is equivalent to calculating the corresponding Green's functions using linear transport theory.² Note that $P(\mathbf{r}_0 \rightarrow \mathbf{r}')$ is directly proportional to the photon fluence rate at \mathbf{r}' and can be denoted as $\phi(\mathbf{r}')$. If we model the absorbing need as a negative line segment source, the fluence rate at \mathbf{r}' can actually be considered the superposition of fluence due to two sources; the first source is a point source corresponding to the source optical fiber, and the second source is a line segment source corresponding to the absorbing needle. The fluence rate of an isotropic point source in a highly scattering at \mathbf{r}' can be given by

$$\phi_S(\mathbf{r}') = \frac{\exp[-\mu_{\text{eff}}|\mathbf{r}' - \mathbf{r}_0|]}{|\mathbf{r}' - \mathbf{r}_0|}, \quad (2)$$

where μ_{eff} is the effective attenuation constant,^{2,7} $\mu_{\text{eff}} = [3\mu_a(\mu_a + \mu_s')]^{1/2}$. The absorbing needle can be considered a negative source used in a similar manner to image sources used for plane geometries. Because of the linear nature of the diffusion equation, the line segment source's Green's function can be constructed by integrating the Green's function of a point source over a line segment,¹² multiplied by a term that accounts for the linear intensity density [in this case, $\rho(\mathbf{l}')$], which results in

$$\phi_N(\mathbf{r}') = \int_{\mathbf{r}_0}^{\mathbf{r}_d} \rho(\mathbf{l}') \frac{\exp[-\mu_{\text{eff}}|\mathbf{r}' - \mathbf{l}'|]}{|\mathbf{r}' - \mathbf{l}'|} d\mathbf{l}', \quad (3)$$

where $\rho(\mathbf{l}')$ is a linear density function of the source intensity. Since the absorbing needle cannot emit more negative photons than real photons that collide with it, we hypothesize that $\rho(\mathbf{l}')$ is dependent on the fluence through the needle at \mathbf{l}' due to the positive point source. If the reflectivity is constant along the length of the needle between the source and detector, then $\rho(\mathbf{l}')$ has the form

$$\rho(\mathbf{l}') = \phi_S(\mathbf{r}') \frac{q_N}{|\mathbf{r}_d - \mathbf{r}_0|}. \quad (4)$$

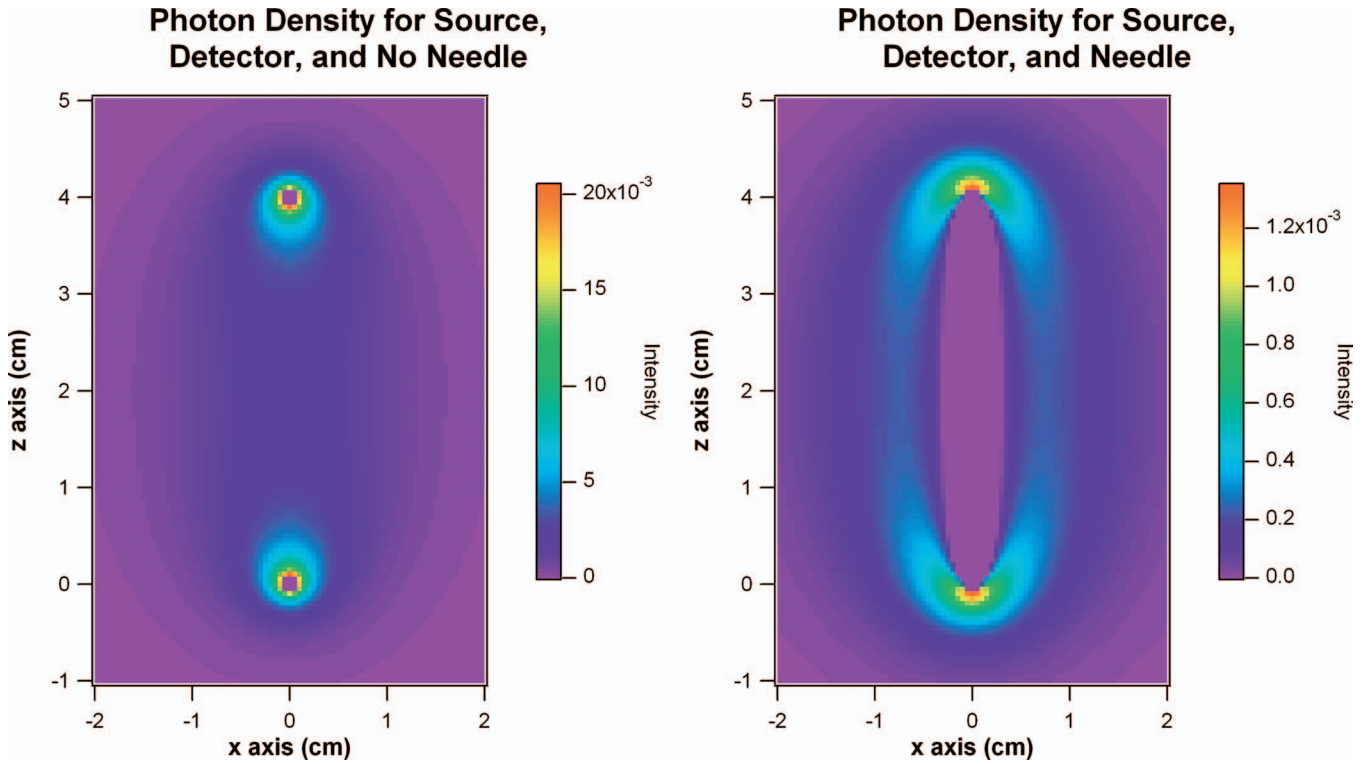


Fig. 1 Plot of $\phi_S(x, 0, z)E_S(x, 0, z)$, left, demonstrates what the PSDF would look like without the influence of the light-absorbing needle. On the right is the plot of $\phi(x, 0, z)E(x, 0, z)$ corresponding to the diffusion approximation for the absorbing needle. In these two plots $L=4$ cm, $\mu_a=0.05$ cm $^{-1}$, and $\mu_s=8$ cm $^{-1}$. Pixels near the source and detector were set to zero (to make the scale such that viewing the changes in the rest of the PSDF easier).

If we choose to place our point source at the origin and the detector at $(0, 0, L)$, and if we connect those two points with a line segment that represents the absorbing needle, Eqs. (2) and (3) can be rewritten as

$$\phi_S(x, y, z) = \frac{\exp[-\mu_{\text{eff}}(x^2 + y^2 + z^2)^{1/2}]}{(x^2 + y^2 + z^2)^{1/2}}, \quad (5a)$$

$$\begin{aligned} \phi_N(x, y, z) &= \phi_S(x, y, z) \\ &\times \int_0^L \frac{q_N \exp\{-\mu_{\text{eff}}[x^2 + y^2 + (z-l)^2]^{1/2}\}}{L [x^2 + y^2 + (z-l)^2]^{1/2}} dl. \end{aligned} \quad (5b)$$

The total fluence at \mathbf{r}' is then

$$\phi(x, y, z) = \phi_N(x, y, z) + \phi_S(x, y, z) \quad (5c)$$

The second probability function that we must calculate that corresponds to $P(\mathbf{r}' \rightarrow \mathbf{r}_d)$ is the escape function. The escape function $E(\mathbf{r}' \rightarrow \mathbf{r}_d)$ is proportional to the fluence rate at the detector. If we now consider there to be a point source at \mathbf{r}' , the derivation of $E(\mathbf{r}' \rightarrow \mathbf{r}_d)$ is equivalent to the derivation of $\phi(\mathbf{r}')$ and is given by

$$E_S(x, y, z) = \frac{\exp\{-\mu_{\text{eff}}[x^2 + y^2 + (L-z)^2]^{1/2}\}}{[x^2 + y^2 + (L-z)^2]^{1/2}}, \quad (6a)$$

$$E_N(x, y, z) = E_S(x, y, z) \int_0^L \frac{q_N \exp(-\mu_{\text{eff}}|L-l|)}{L |L-l|} dl, \quad (6b)$$

$$E(x, y, z) = E_S(x, y, z) + E_N(x, y, z). \quad (6c)$$

The visitation density function is then proportional to $\phi(x, y, z) E(x, y, z)$. The careful observer will notice that the integral in Eq. (6b) blows up at the end points and is not descriptive of reality; however, the integral is constant for a given problem setup. In our numerical calculations, the integral is simply replaced by a constant that does not include integration near the endpoints.

Using numerical methods, it is possible to produce density plots that demonstrate how changing the reflectivity changes the sensitive volume of the optical needle (see Fig. 1). Doing so demonstrates that the introduction of an absorbing needle shifts the average photon path away from the needle, while absence of the needle allows the average photon path to follow a straight path from source to detector.

In our technique, the needle is used as support for the optical fibers to perform a 1-D tomography of the needle surroundings. For our method to work, we require relatively large source-detector separations, since our purpose is to explore the volume relatively far from the needle. (For the semi-infinite geometry, increasing the source, detector separation distance increases the average depth of tissue visited by photons in diffuse reflectance measurements.¹⁴) However, the

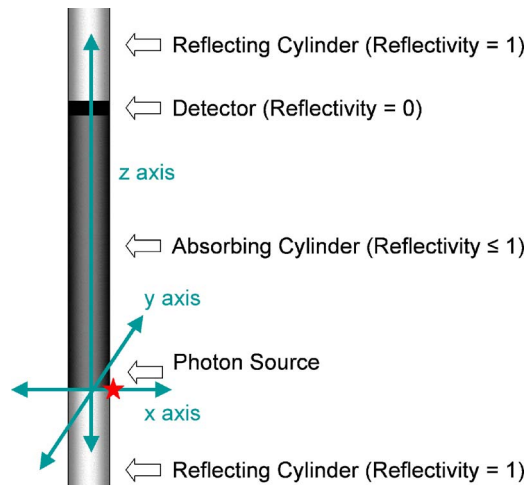


Fig. 2 Monte Carlo needle setup. The cylinder representing the needle had a radius of 3 cm. The absorbing cylinder part had a length of 4 cm, and the detector had a length of 0.2 cm. The photons were launched from the side of the needle cylinder at the base of the absorbing cylinder, initially propagating in the x direction.

concept of having an absorbing needle will influence the light density also if the source-detector distance is a few millimeters. The size of this effect depends on the regime of light transport. If there is multiple scattering, the absorbing material of the needle will have an effect.

3 Monte Carlo Simulations

3.1 Description of the Monte Carlo Model Geometry

For our Monte Carlo simulations, we modeled the optical needle as being broken up into four sections. The absorbing needle section was modeled as a hard cylinder, 4 cm long, pointing along the z axis. The detector was also modeled as a hard cylinder, 0.2 cm long, and it was placed at the end of the needle's cylinder. Two totally reflecting, semiinfinitely long hard cylinders were placed before the absorbing needle and after the detector cylinder so that all the cylinders were aligned and were of equal radius (0.3 cm), making one long "needle" (see Fig. 2).

Photons were injected at a point at the bottom edge of the absorbing needle cylinder with an initial propagation direction along the x axis. We used absorption and scattering coefficients of 0.05 and 8 cm^{-1} , respectively; these values are similar to those of brain and breast tissue.^{3,15} Photons were propagated through the "tissue" isotropically.^{4,14,16} Frequency domain information was collected using the modified shortcut method described by Testorf et al.¹⁷ A slightly different setup was used to measure radius dependence (the radius varied, and the reflection off of the cylinder was diffuse instead of specular).

3.2 Construction of the PSDFs

The simulation programs were written in C++ and modeled after the popular MCML program used for photon-tissue simulations.^{4,18} PSDFs were³ constructed by counting collisions in voxels that were essentially concentric, hollow cylinders. The voxels were 1 mm in length along the z axis of the

needle cylinder, and the inner surface of each concentric ring was 1 mm away from the inner surface of the ring just inside of it. The resulting number of counts in each ring voxel was divided by the volume of the voxel to give a PSDF that is related to the density of photons in a plane that cuts through the z axis of the needle.

3.3 Photon Path Dependence on Needle Reflectivity

PSDFs were constructed to compare the average photon paths for several needle reflectivities (Fig. 3). The needle reflectivity was modeled by calculating a specular reflection off of the needle and assigning a probability of reflection by the needle. A successive collision with the needle would produce a new value for the probability of reflection, and if the new value was less than the previous, then the value was updated. If the photon eventually reached the detector, an object containing a linked list of the photon's history was passed to an object that updated data arrays for the photon density and phase. PSDFs were constructed for several reflectivity values, and the relative drop in total intensity was also recorded. The results demonstrated that a totally reflective needle (reflectivity=1) has a PSDF similar to the PSDF of a point source and detector in an infinite medium, as found by the diffusion equation, and a totally absorbing needle (reflectivity=0) has a PSDF similar to our model diffusion approximation photon density function. Intermediate values of reflectivity had PSDFs that varied between the two extremes. Also note that the overall intensity drops as the reflectivity is decreased (Fig. 4).

3.4 Photon Path Dependence on Needle Radius

Monte Carlo data was also collected for several different needle radii. It became apparent that as the radius of the needle increases, the distance away from the edge of the needle at which the maximum photon density is found also increases. The rate of change seems to be largest for small radii. Also, the intensity of photons is seen to decrease at the maximum (Fig. 5).

4 Experimental

4.1 Materials and Methods

4.1.1 Equipment

To verify the results of the diffusion approximations and Monte Carlo simulations that describe the average photon path from source to detector, we used a three-axis table micropositioner, a scattering medium (2% milk), and a laser diode and two photomultiplier tube (PMT) channels of an ISS frequency domain tissue oximeter (Oximeter, ISS, Champaign, Illinois). We used 2% milk fat milk for the scattering medium because it does not have the settling problems of TiO_2 mixtures,² has scattering and absorption coefficients similar to human tissues,⁷ and perhaps most importantly, is readily available. The laser diode is modulated at a frequency of 110 MHz, and the second dynode of the PMTs is modulated at 110.005 MHz to demodulate the high frequency.⁵ The laser diode light (670 nm) was conducted to and from the milk through optical fibers. Part of the detector fiber was colored black or white as a means to change the reflectivity of the needle. We measured the positional influence of a small, black target object on the intensity and phase lag of light

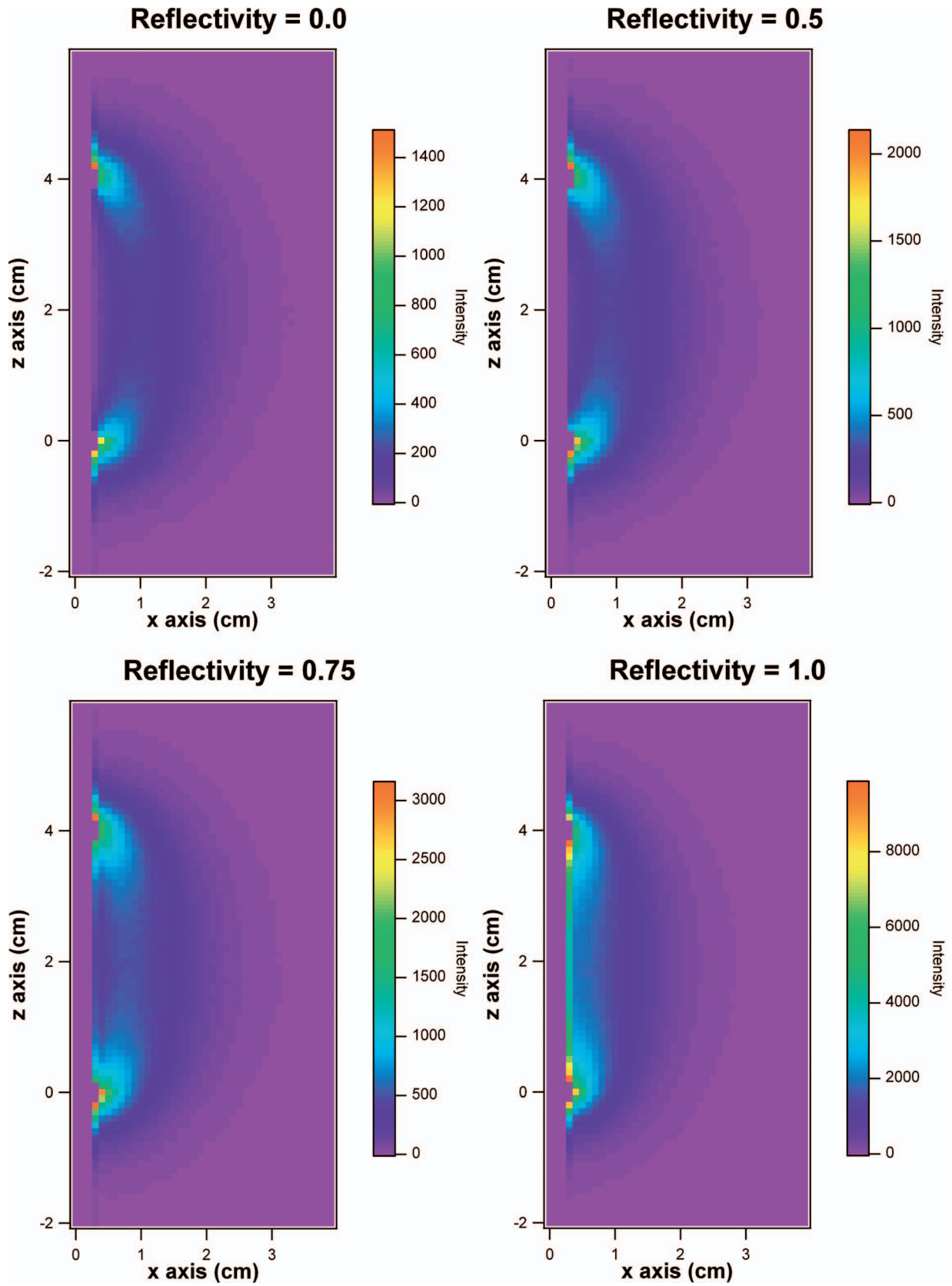


Fig. 3 Monte Carlo PSDFs with needle reflectivity=0, 0.5, 0.75, and 1.0. Pixels associated with the source and detector were set to zero (to make the scale such that viewing the changes in the rest of the PSDF easier).

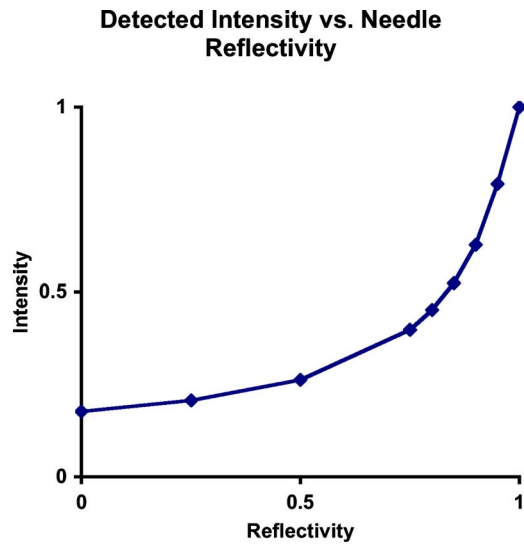


Fig. 4 Intensity as a function of reflectivity based on Monte Carlo absorbing needle simulations. Here the source-detector separation was 4 cm, and the needle radius was 0.3 cm.

reaching the distal detector by moving the target through the milk using the micropositioner. See Fig. 6 for a representation of the setup.

4.1.2 Spatial intensity measurement

Measurements were taken in a raster fashion for positions of the black target relative to the black needle. The small black target is the absorption object used to probe the photon density. It is assumed that if the detected light intensity goes down more when the black target moves into one particular region of space than it does when the target moves into a different region of space, then the photon density in the first region of space is greater. Hence, we use the positioning of

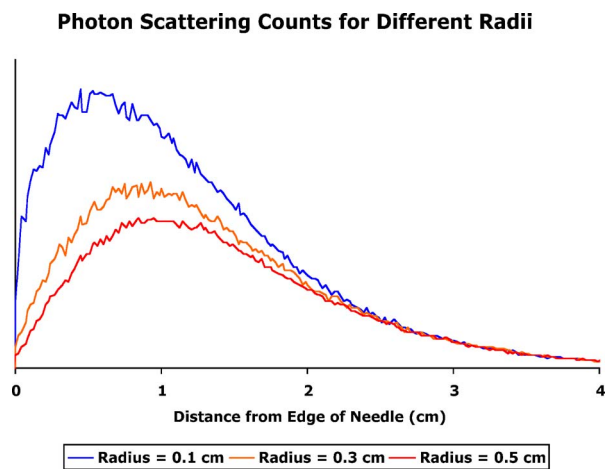


Fig. 5 Comparison of Monte-Carlo-generated photon scattering as a function of distance away from perfectly absorbing needles that vary in the size of their radii. The number of photons reaching the detector for each radius is scaled to $n=1000$. Distance away from edge of needle is measured as the radial distance from the lengthwise center of the absorbing needle. The number of counts has also been scaled for increasing voxel-size dependence on radius.

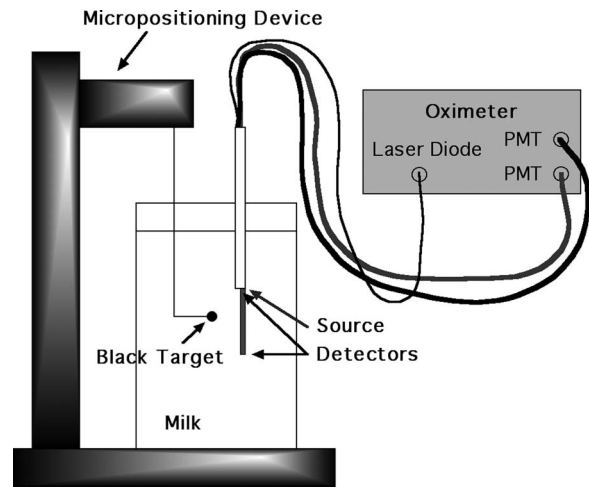


Fig. 6 Experimental setup. The raster scanning device moves a black target through the x-z plane where the black needle (in this case, the blackened end of a fiber optic) is pointing along the z axis. The light source and detectors are part of an ISS oximeter (ISS, Champaign, Illinois) with a laser diode source (630 nm) and PMT detectors. For the intensity measurements, light intensity was measured at the distal end of the needle. The phase measurements used both detectors, the detector near the light source being the reference detector.

the black target to map out the photon density. Optical fibers connected to the oximeter were inserted into the milk. The end of the detector's fiber optic cable was colored black with a black marker to simulate an absorbing needle (reflectivity = 0). The end of the fiber optic leading from the laser diode was positioned four centimeters above the end of the detector fiber optic, and white tape held the two optical fibers together. Black cloth was placed around the setup to minimize noise from the room lights. The black target was attached to the micropositioner through a transparent capillary tube. This black target was moved in a raster fashion along the length of and away from the "needle" to produce a two dimensional map of the influence of the target position on the intensity of light reaching the detector (Fig. 7, right).

To verify that the average photon path shifts closer to more reflective needles, white tape was placed around the "black needle." Another image was collected (Fig. 7, left). It was seen that the image thus created was similar to the image produced by the simple analytical model for source and detector in the absence of a black needle (Fig. 1) and the totally reflective Monte Carlo simulation (Fig. 3).

4.1.3 Spatial phase lag measurement

To measure the spatial influence of the black target on the phase lag, a reference detector fiber optic was placed next to the source, in addition to the detector found at the distal end of the black needle. The "black needle" length was reduced to 3.5 cm in this experiment so that more light would reach the detector and thus reduce the shot noise (with the expectation that the phase lag is a much more sensitive measurement). The light source was again modulated at 110 MHz. Frequency domain information was collected for both detector channels. The difference between the phases of the signals in both channels was considered the phase lag. It is assumed that as the target moves into volume elements with higher photon

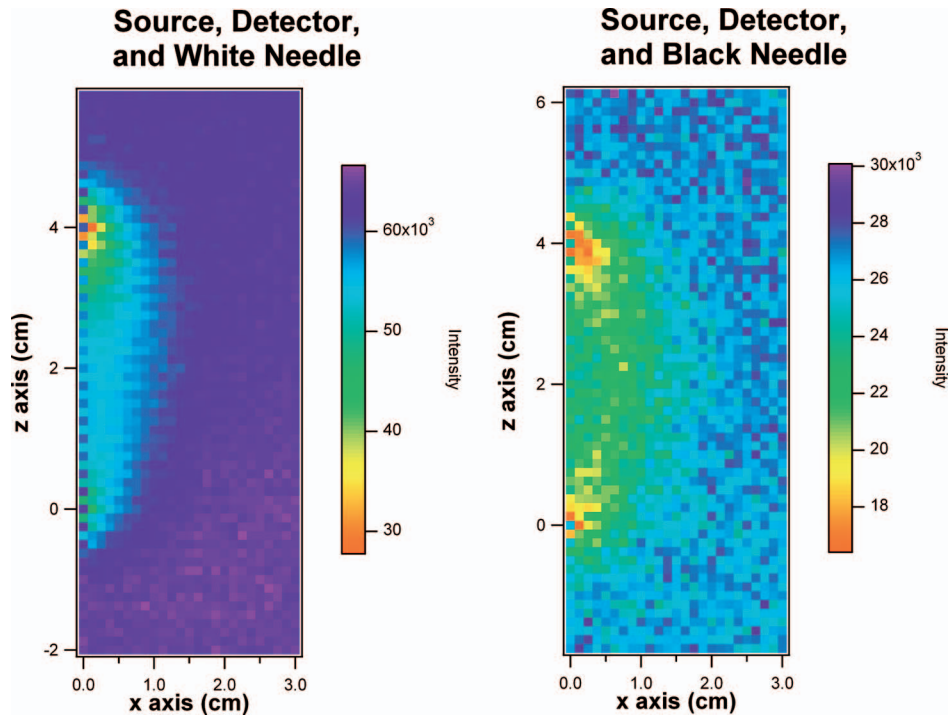


Fig. 7 Left: Image produced by placing white tape around the “black needle.” This was done to verify that, for more reflective needles, the average photon path is shifted nearer to the needle. Right: Observed changes in photon count for a raster scan in the x-z plane. The blackened “needle” is directed along the z axis and is found near the left edge of the image. This image shows the expected shift of the photon path away from the needle. The source-detector separation distance is 4 cm for both images. Compare with the Monte Carlo results in Fig. 3.

visitation probabilities, the average total path length for a photon to reach the distant detector must change because the average path of the photons is significantly changed. The results showed that the phase lag increases as the black target crosses the average photon path (Fig. 8).

4.2 Results

Figure 7 maps light intensity reaching the detector for positions of the target relative to the needle. It is assumed that the amount of light reaching the detector is less when the black object is found impeding the average path of photons through the scattering medium. If this is indeed the case, then Fig. 7, right, clearly demonstrates that the most-visited volume elements are found at distances well away from the needle. Figure 7, left, is the result of the control experiment: when white tape is placed around the exterior of the black needle, the intensity map appears to be more like what is to be expected for a source and a detector in an infinite medium without a black needle. Thus, Fig. 7 demonstrates that the presence of the black needle does indeed change the average path of photons that leave the source, pass through the milk, and arrive at the detector.

5 Detection of Inhomogeneities

To test the usefulness of the needle in detecting tissue inhomogeneities, we wrote a Monte Carlo simulation that introduced inhomogeneities. This Monte Carlo simulation was the same as our simulation described in Sec. 3.3, except we introduced a second layer of tissue around the tissue that sur-

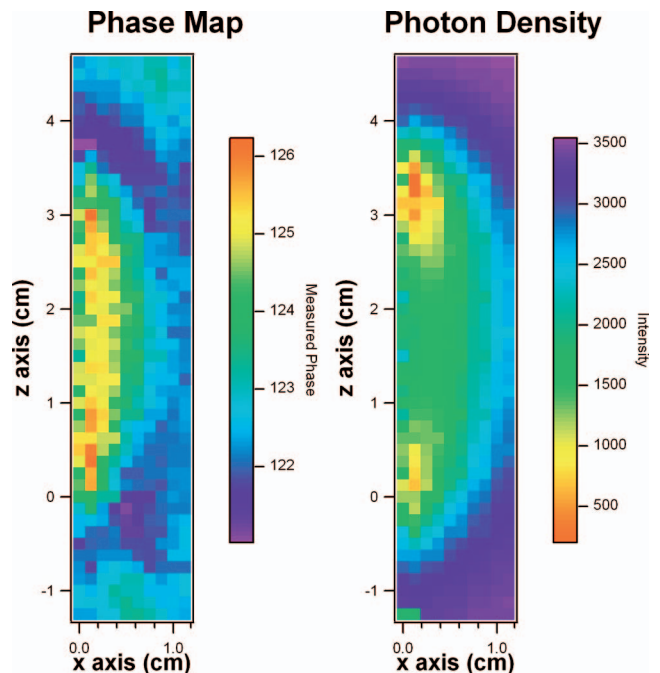


Fig. 8 Left: Map of the phase dependence on the position of the black target for the black needle. Right: corresponding intensity dependence on the position of the black target for the same experiment. Source-detector separation is 3.5 cm. By inspection we can see that the phase lag has a spatial dependence similar to that of the intensity.

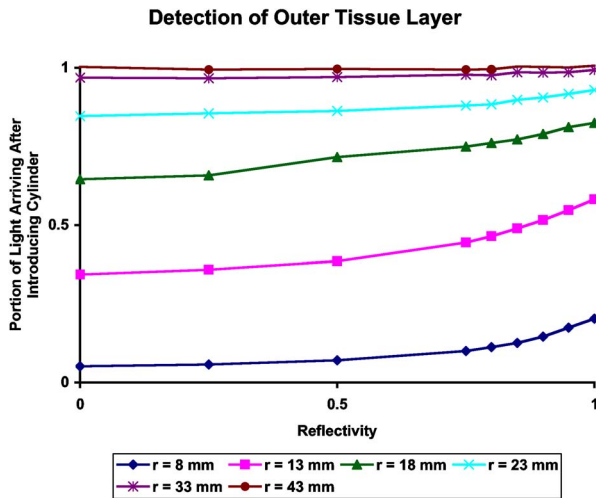


Fig. 9 Graph demonstrating how changing the reflectivity of the needle changes the intensity of light arriving at the detector when a second, cylindrical layer of tissue is introduced around the needle. The radii at which the boundary between the two layers is found is indicated in the legend at the bottom of the figure.

rounded the absorbing needle. This new layer of tissue was given scattering and absorption coefficients double the values of the coefficients of the original tissue. The two layers of tissue were separated by a cylindrical boundary. We varied both the reflectivity of the needle and the radius of the cylindrical boundary between the two tissue layers. The intensities of light detected after the second tissue layer was introduced were compared with the detected light intensities before the second layer was introduced. When the tissue boundary was far from the needle, there was little or no change in the ratio of the intensity with or without the tissue inhomogeneity. When the inhomogeneity boundary was closer to the needle, the ratio of the intensity with and without the inhomogeneity changed significantly with respect to needle reflectivity. This demonstrates that modulating the needle reflectivity makes detection of inhomogeneities at different radial distances possible. See Fig. 9.

All our experiments were done with needles of different reflectivity. However, we plan to change the reflectivity by designing a needle with an external jacket that can be rotated to change the surface reflectivity. Thus, in practice we will be able to modulate the reflectivity of the needle in situ, even though we do not show it here.

6 Summary, Discussion, and Conclusions

We showed through diffusion approximations, Monte Carlo simulations, and direct experiment that the average photon path changes as the reflectivity of an optical needle changes. It is clear that as reflectivity decreases, the average photon path for photons reaching the detector shifts away from the absorbing needle. Experiments also indicate that modeling the optical needle as a negative photon line segment source gives qualitative results that compare well with Monte Carlo simulations and experiment.

We effectively presented a method to alter photon paths by modulating the reflectivity of an absorbing needle; however,

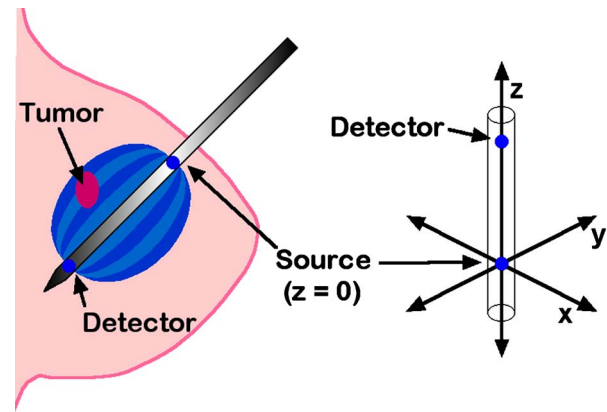


Fig. 10 Proposed insertion of needle into breast tissue for 1-D tomography. The source and detector are both located along the z axis of the needle. When the reflectivity of the needle is changed, the average photon path is shifted away from the needle. This is depicted on the left as shells of light densities that correspond to different reflectivities. By changing the reflectivity of the needle, tissue can be measured at varying radii away from the needle.

the method could also be applied to other geometries. The optical needle is particularly useful for medical applications because it is minimally invasive but can still reach many parts of the body. Selectivity in the reflectivities of optical needles should make it possible to manufacture a variety of needles doctors can choose from to select the most appropriate sensitive volume for a given application. Perhaps more exciting, though, is that the modulation of reflectivity of optical needles opens the door for internal, site-specific optical tomography, which could be useful in breast cancer diagnosis (Fig. 10). By gradually changing the reflectivity of an optical needle, it is possible to change the average photon path, and hence, the volume of tissue explored. This opens the door for internal optical tomography, which may be useful in cases when optical tomography measurements taken by placing source and detector on the skin are not sufficient.

Acknowledgments

This research was jointly supported by National Institutes of Health (NIH) PHS 9ROI, Grant No. EB00559, and NIH, NTROI-1U54CA105480-01.

References

1. C. Lubawy and N. Ramanujam, "Endoscopically compatible near-infrared photon migration probe," *Opt. Lett.* **29**, 2022–2024 (2004).
2. M. S. Patterson, S. Anderson-Engels, B. C. Wilson, and E. K. Osei, "Absorption spectroscopy in tissue-simulating materials: a theoretical and experimental study of photon paths," *Appl. Opt.* **34**, 22–30 (1995).
3. F. Bevilacqua, J. S. You, C. K. Hayakawa, and V. Venugopalan, "Sampling tissue volumes using frequency-domain photon migration," *Phys. Rev. E* **69**, 051908 (2004).
4. L. Wang, S. L. Jacques, and L. Zheng, "MCML—Monte Carlo modeling of light transport in multi-layered tissues," *Comput. Methods Programs Biomed.* **47**, 131–146 (1995).
5. S. A. Walker, D. A. Boas, and E. Gratton, "Photon density waves scattered from cylindrical inhomogeneities: theory and experiments," *Appl. Opt.* **37**, 1935–1944 (1998).
6. S. Fantini, M. A. Franceschini, and E. Gratton, "Semi-infinite-geometry boundary problem for light migration in highly scattering media: a frequency-domain study in the diffusion approximation," *J.*

- Opt. Soc. Am. B* **11**, 2128–2138 (1994).
7. J. B. Fishkin and E. Gratton, "Propagation of photon-density waves in strongly scattering media containing an absorbing semi-infinite plane bounded by a straight edge," *J. Opt. Soc. Am. A* **10**, 127–140 (1993).
 8. J. S. Maier, S. Walker, and E. Gratton, in *Biomedical Optical Instrumentation and Laser-Assisted Biotechnology*, pp. 121–142 (1996).
 9. M. S. Patterson, B. Chance, and B. C. Wilson, "Time resolved reflectance and transmittance for the non-invasive measurement of tissue optical properties," *Appl. Opt.* **28**, 2331–2323 (1989).
 10. S. Fantini, M. A. Franceschini-Fantini, J. S. Maier, S. Walker, B. Barbieri, and E. Gratton, "Frequency-domain multichannel optical detector for noninvasive tissue spectroscopy and oximetry," *Opt. Eng.* **34**, 32–42 (1995).
 11. M. Wolf, U. Wolf, J. H. Choi, V. Toronov, L. A. Paunescu, A. Michalos, and E. Gratton, "Fast cerebral functional signal in the 100-ms range detected in the visual cortex by frequency-domain near-infrared spectrophotometry," *Psychophysiology* **40**, 521–528 (2003).
 12. K. M. Case and P. F. Zweifel, *Linear Transport Theory*, Addison-Wesley, Reading, MA (1967).
 13. M. L. Shendeleva, "Green functions for diffuse photon-density waves generated by a line source in two nonabsorbing turbid media in contact," *Appl. Opt.* **43**, 1638–1642 (2004).
 14. G. H. Weiss, R. Nossal, and R. F. Bonner, "Statistics of penetration depth of photons re-emitted from irradiated tissue," *J. Mod. Opt.* **36**, 349–359 (1989).
 15. W. F. Cheong, S. A. Prahl, and A. J. Welch, "A review of the optical properties of biological tissues," *IEEE J. Quantum Electron.* **26**, 2166–2185 (1990).
 16. S. A. Dupree and S. K. Fraley, *A Monte Carlo Primer: A Practical Approach to Radiation Transport*, Kluwer Academic/Plenum Publishers, New York (2002).
 17. M. Testorf, U. Osterberg, B. Pogue, and K. Paulsen, "Sampling of time- and frequency-domain signals in Monte Carlo simulations of photon migration," *Appl. Opt.* **38**, 236–245 (1999).
 18. S. L. Jacques and L. Wang, in *Optical-Thermal Response of Laser-Irradiated Tissue*, A. J. Welch and M. J. C. van Gemert, Eds., pp. 73–100, Plenum Press, New York (1995).